First determination of ground state electromagnetic moments of ^{53}Fe

A. J. Miller,[1,2,*] K. Minamisono,[1,2,†] D. M. Rossi,[3] R. Beerwerth,[4,5] B. A. Brown,[1,2] S. Fritzsche,[4,5] D. Garand,[1] A. Klose,[6] Y. Liu,[7] B. Maaß,[3] P. F. Mantica,[8,9] P. Müller,[10] W. Nörtershäuser,[3] M. R. Pearson,[11] and C. Sumithrarachchi[1]

[1]*National Superconducting Cyclotron Laboratory, Michigan State University, East Lansing, Michigan 48824, USA*
[2]*Department of Physics and Astronomy, Michigan State University, East Lansing, Michigan 48824, USA*
[3]*Institut für Kernphysik, Technische Universität Darmstadt, 64289 Darmstadt, Germany*
[4]*Helmholtz-Institut Jena, 07743 Jena, Germany*
[5]*Theoretisch-Physikalisches Institut, Friedrich-Schiller-Universität Jena, 07743 Jena, Germany*
[6]*Department of Chemistry, Augustana University, Sioux Falls, South Dakota 57197, USA*
[7]*Physics Division, Oak Ridge National Laboratory, Oak Ridge, Tennessee 37831, USA*
[8]*Facility for Rare Isotope Beams, Michigan State University, East Lansing, Michigan 48824, USA*
[9]*Department of Chemistry, Michigan State University, East Lansing, Michigan 48824, USA*
[10]*Physics Division, Argonne National Laboratory, Lemont, Illinois 60439, USA*
[11]*TRIUMF, Vancouver, British Columbia V6T 2A3, Canada*

(Received 22 September 2017; published 16 November 2017)

The hyperfine coupling constants of neutron deficient ^{53}Fe were deduced from the atomic hyperfine spectrum of the $3d^6 4s^2\ ^5D_4 \leftrightarrow 3d^6 4s 4p\ ^5F_5$ transition, measured using the bunched-beam collinear laser spectroscopy technique. The low-energy ^{53}Fe beam was produced by projectile-fragmentation reactions followed by gas stopping, and used for the first time for laser spectroscopy. Ground state magnetic-dipole and electric-quadrupole moments were determined as $\mu = -0.65(1)\,\mu_N$ and $Q = +35(15)\ e^2\text{fm}^2$, respectively. The multiconfiguration Dirac-Fock method was used to calculate the electric field gradient to deduce Q from the quadrupole hyperfine coupling constant, since the quadrupole coupling constant has not been determined for any Fe isotopes. Both experimental values agree well with nuclear shell model calculations using the GXPF1A effective interaction performed in a full fp shell model space, which support the soft nature of the ^{56}Ni nucleus.

DOI: 10.1103/PhysRevC.96.054314

I. INTRODUCTION

Variation of shell gaps due to the shifts of single-particle energy levels leads to an appearance and disappearance of magic numbers, which has now been established in several regions of the nuclear chart [1–4]. The shifts are particularly evident for nuclei with large proton-neutron imbalances [5]. The ^{56}Ni nucleus with neutron and proton numbers $N = Z = 28$ is the first self-conjugate and doubly magic nucleus that occurs due to a shell gap driven by the spin-orbit force. Studies of the ^{56}Ni nucleus and its neighboring nuclides provide critical insight into the structure of doubly magic nuclei as one moves away from the β-stability line in the nuclear chart and have revealed a soft nature of the ^{56}Ni nucleus [6].

The magnetic-dipole moment is a sensitive probe of the nucleon configuration inside a nucleus. The magnetic moments of nuclei one nucleon away from ^{56}Ni provide important insight into the structure of ^{56}Ni, since shell model calculations are straightforward with an assumption of ^{56}Ni being an inert core, and any deviation signals an abnormal structure. Magnetic moments of the odd nucleon nuclei ^{55}Ni [7], ^{55}Co [8], ^{57}Cu [9], and ^{57}Ni [10] around ^{56}Ni are all known and require large-scale shell model calculations in the full fp shell-model space [11] to reproduce the experimental values, where the ^{56}Ni core is open to allow particle-hole excitations. These good agreements indicate a soft nature of ^{56}Ni, because the calculated probability of the $N = Z = 28$ lowest-order closed shell configuration is only 60%, compared to a 90% closed shell component in the wave function of the ^{48}Ca ground state.

The ground state electromagnetic moments of ^{53}Fe in the vicinity of ^{56}Ni were determined from the atomic hyperfine structure using the collinear laser spectroscopy (CLS) technique. The charge radii of neutron-deficient ^{52,53}Fe isotopes were also determined, and have been reported elsewhere [12], where the apparent similarity of the Fe and Ca kink structures at $N = 28$ in the chain of charge radii are presented. In this paper, the ground state nuclear moments of ^{53}Fe are discussed.

Low-emittance, low-energy (∼30 keV) ^{53}Fe beams for the CLS measurement were produced through projectile-fragmentation reactions and subsequent in-flight separation [13] followed by gas stopping [14]. This procedure to prepare radioactive beams was employed for the first time for bunched-beam collinear laser spectroscopy measurements in the present study.

The Fe isotopes are known to be notoriously difficult to produce at isotope separator on line (ISOL) facilities, where many laser spectroscopy data have been obtained for selected elements [15]. At these facilities, rare isotopes are extracted from thick targets bombarded by light ions. Long chains of isotopes have been systematically investigated, taking advantage of the low-emittance, low-energy beams (∼60 keV) and the high beam intensities available for many nuclides of certain elements. The number of elements, for which rare isotopes can be produced with the ISOL technique, is limited when long release times from the targets lead to large decay losses. These limitations have been partly overcome by the ion guide at an isotope separator on line (IGISOL) approach,

*Corresponding author: millera@nscl.msu.edu
†Corresponding author: minamiso@nscl.msu.edu

where low-energy reaction products are stopped in a gas and converted into a low-energy ion beam [16]. On the other hand, the current scheme of stopped beams from in-flight production can be applied for isotopes of all elements lighter than uranium, and complements the capabilities of the other facilities. This leads to new opportunities for laser spectroscopy to explore elements that are difficult to produce at ISOL facilities and nuclei far from the β-stability line.

It is noted that no ground state quadrupole moment or hyperfine quadrupole coupling constant has been reported so far for any Fe isotope. This is due to the existence of only one odd-mass stable Fe isotope, ^{57}Fe, whose nuclear spin is $1/2$ and therefore lacks the quadrupole interaction. Also the electronic structure of the Fe atom is complex and challenging to calculate an electric field gradient, which is required to deduce nuclear quadrupole moments from hyperfine quadrupole coupling constants. It is shown in the present study that the multiconfiguration Dirac-Fock (MCDF) method can be applied to reliably compute atomic factors of the Fe atom to deduce nuclear structure information.

A brief introduction to the hyperfine interaction is presented in Sec. II. Details of the experiment are given in Sec. III, followed by the results in Sec. IV. The results are discussed in Sec. V, including comparison with shell model calculations and a prediction for the magnetic moment of the mirror nucleus ^{53}Co through the Buck-Perez relation [17]. An inferred value of the isoscalar spin expectation value for the mass $A = 53$ system is also discussed.

II. HYPERFINE INTERACTION

The shift of an atomic energy level due to the hyperfine interaction relative to an atomic fine-structure level is given by

$$\Delta E = \frac{K}{2} A^{\mathrm{HF}} + \frac{3K(K+1) - 4I(I+1)J(J+1)}{8I(2I-1)J(2J-1)} B^{\mathrm{HF}} \quad (1)$$

with $K = F(F+1) - I(I+1) - J(J+1)$, where F is the quantum number associated with the total angular momentum of the atom, defined by $\mathbf{F} = \mathbf{I} + \mathbf{J}$. Here, I and J are the total angular momenta/spins of the nucleus and electrons, respectively. A^{HF} and B^{HF} are the hyperfine coupling constants defined as

$$A^{\mathrm{HF}} = \frac{\mu B(0)}{IJ}, \quad (2)$$

$$B^{\mathrm{HF}} = eQ\left\langle \frac{\partial^2 V_e}{\partial z^2} \right\rangle, \quad (3)$$

where μ is the nuclear magnetic-dipole moment, $B(0)$ is the magnetic field generated by the atomic electrons at the center of the nucleus, e is the electric unit charge, Q is the spectroscopic nuclear electric-quadrupole moment, and $\langle \partial^2 V_e/\partial z^2 \rangle \equiv q$ is the electric field gradient produced by the atomic electrons at the center of the nucleus. The magnetic field and the electric field gradient are isotope independent assuming a point-like nucleus (the hyperfine anomalies [18] are neglected here). According to Eqs. (2) and (3), unknown nuclear moments may be deduced from the measured hyperfine coupling constants using a reference nucleus of the same element whose hyperfine coupling constants for the same electronic level and nuclear moments are known. A simple ratio of hyperfine coupling constants derives nuclear moments as

$$\mu = \mu_{\mathrm{R}} \frac{A^{\mathrm{HF}}}{A_{\mathrm{R}}^{\mathrm{HF}}} \frac{I}{I_{\mathrm{R}}}, \quad (4)$$

$$Q = Q_{\mathrm{R}} \frac{B^{\mathrm{HF}}}{B_{\mathrm{R}}^{\mathrm{HF}}}, \quad (5)$$

where the subscript R indicates a reference nucleus whose electromagnetic moments, nuclear spin and hyperfine coupling constants are known. If a suitable reference isotope does not exist, the magnetic field and electric field gradient have to be evaluated theoretically.

III. EXPERIMENT

The radioactive ^{53}Fe($T_{1/2} = 8.52$ m; $I^{\pi} = 7/2^{-}$) ion beam was produced by fragmentation of a stable ^{58}Ni beam on a $^{\mathrm{nat}}$Be target. The ^{58}Ni primary beam was accelerated to 160 MeV/nucleon in the coupled cyclotrons at National Superconducting Cyclotron Laboratory (NSCL) at Michigan State University.

The ^{53}Fe beam was separated from other reaction products through the A1900 fragment separator [13], thermalized in a large-volume, helium-filled gas cell [14], and extracted by RF and DC electric fields as singly charged ions at an energy of 30 keV. The isomeric state in ^{53}Fe, $^{53\mathrm{m}}$Fe($T_{1/2} = 2.5$ m; $I^{\pi} = 19/2^{-}$) at an excitation energy of 3.04 MeV, was also populated in the production process in addition to the ground state of interest. The production ratio of the isomeric component to the ground state was determined by collecting the low-energy Fe beam on a foil and detecting characteristic γ rays from the isomeric and ground states. The ratio obtained was $^{53\mathrm{m}}\mathrm{Fe}/^{53}\mathrm{Fe} = 0.050(2)$.

A low-energy Fe^{+}-ion beam at an energy of 30 keV was transported to the beam cooler and laser spectroscopy (BECOLA) facility [19,20], where the beam was injected into a radio frequency quadrupole (RFQ) cooler/buncher [21] filled with helium buffer gas. A schematic of the BECOLA facility is shown in Fig. 1. Buffer gas pressures in the RFQ were $\sim$100 mTorr and $\sim$1 mTorr in the cooling and bunching sections, respectively. The injected ion beams were trapped in the RFQ, extracted as ion-beam bunches at a potential of 29 856(4) V, and then transported to the collinear laser spectroscopy (CLS) beam line, where the ion beams were aligned onto the optical axis of the laser light. The extraction voltage was monitored throughout the experiment using a precision voltage divider and 6.5-digit digital voltmeters, as shown in Fig. 1. A 9998.28(67):1 voltage divider (HVS-100 [22]), calibrated to an accuracy of 7×10^{-5} was used to measure the extraction voltage. This read-out voltage was recorded every few seconds to allow a long integration time to obtain maximum accuracy of the digital voltmeter.

The ion-beam bunch was extracted from the RFQ with a repetition rate of 1 Hz, and the bunch width (full width at the half-maximum) was set to $\sim$1 μs without increasing the typical resolution of $\sim$80 MHz of the hyperfine spectrum. The time spectrum of the bunched beam is shown in Fig. 2.

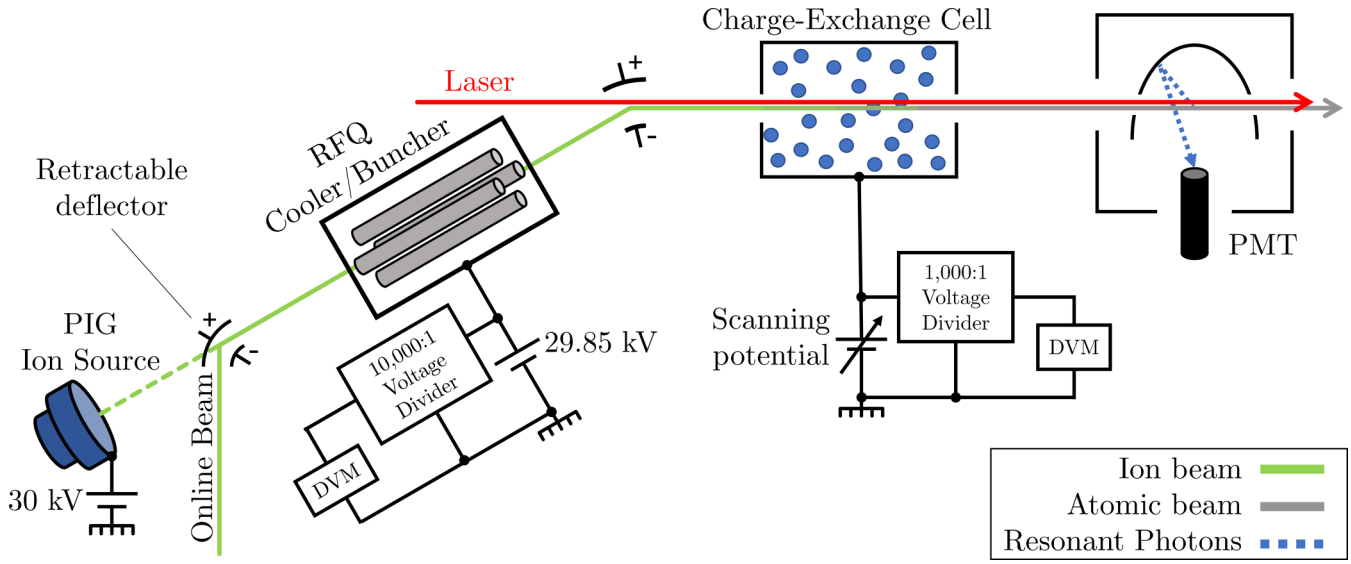

FIG. 1. The BECOLA facility. Fe^+ ions are sent to the RFQ cooler/buncher from either the PIG ion source or the online beam. Following the cooler/buncher, the ion beam is overlapped with the laser light, and sent through a charge-exchange cell (CEC) containing sodium vapor. The laser-resonant fluorescence from the neutral atoms is collected using an elliptical mirror and detected by a photomultiplier tube (PMT). The static potential applied to the RFQ cooler/buncher and the scanning potential applied to the CEC were recorded with high precision using two digital voltmeters (DVMs).

By selecting only photon counts within this time window, background originating from scattered laser light can be dramatically reduced [23,24]. In the present measurement a nominal background suppression factor of 10^6 was achieved.

A charge-exchange cell (CEC) [25] with a sodium vapor was used to neutralize the incoming Fe^+-ion beam for the laser-induced fluorescence measurements on the $3d^6 4s^2\ ^5D_4$; $0.00\,\mathrm{cm}^{-1} \leftrightarrow 3d^6 4s4p\ ^5F_5$; $26\,874.548\,\mathrm{cm}^{-1}$ transition in Fe I at 372 nm [26]. The sodium vapor pressure was adjusted to attain a neutralization efficiency of approximately 50%, as higher values may broaden the resonance line width by inelastic reactions [25,27]. Electronic states are populated through the charge-exchange reactions around the entry energy of an electron, which is defined as the difference of ionization energies (IE) between Na($^2S_{1/2}$) and Fe($^5D_4$); that is IE(Na) − IE(Fe) = $22\,272.1\,\mathrm{cm}^{-1}$. Although the reaction is considered as a semiresonant charge-exchange with some Fe I excited levels being close to the entry energy, many other nonresonant electronic states are also populated around the entry energy due to the high electronic level density of Fe I. The populated excited states can decay toward the ground state before the Fe beam bunch reaches the photon detection system. There was a 40 cm distance between the CEC and the photon detection system, which corresponds to about 1.3 μs flight time for a 30 keV ^{53}Fe beam. A simulation [28] was performed to describe a 29.85 keV Fe^+ beam impinging on a sodium vapor, and the electronic population distribution of neutral Fe at the photon detection system was estimated. The result is shown in Fig. 3. The initial population distribution over the Fe electronic levels right after the CEC is redistributed according to lifetimes and branching ratios, and cascades toward low-lying levels. The results of these simulations indicate that 5% of the total Fe population occupies the $3d^6 4s^2\ ^5D_4$ ground state at the photon detection region. The severe fractionalization of the level population is a common feature of charge-exchange of ions whose electronic level density is high, which then reduces the sensitivity of CLS significantly. The typical atomic beam rates of ^{53}Fe after the CEC relevant to the laser excitation were estimated to be 1500 atoms/s based on the 5% population in the atomic ground state.

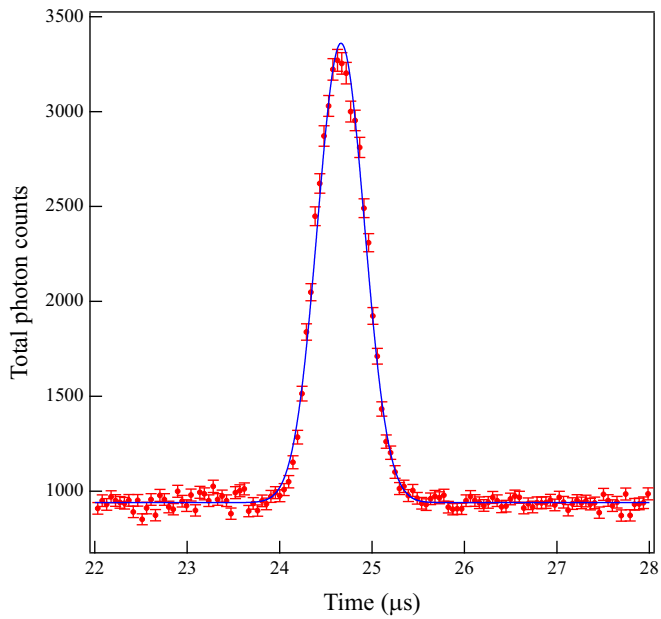

FIG. 2. ^{53}Fe time spectrum as a function of time relative to trigger signals for the release of the ion bunches. This spectrum includes total photon counts over ∼12 h data accumulation time. The time spectrum was measured with a PMT at the photon detection system and includes both resonant photons and non-resonant photons following the charge-exchange process.

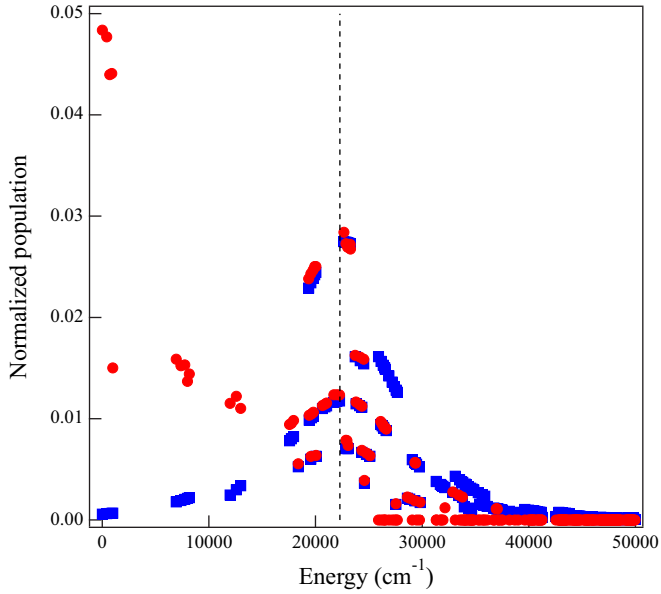

FIG. 3. Simulated population distribution after charge-exchange (CE) of 29.85 keV Fe^{+}-ion beam with a sodium vapor. The horizontal axis shows electronic levels of the Fe atom. Blue squares are the initial distribution right after the CE reactions, red circles are the distribution at the photon detection system 40 cm away from the CEC, and the dashed line is the entry energy of the electron from sodium.

The laser system employed for the CLS measurement was composed of a continuous-wave 532 nm Spectra-Physics diode-pumped solid-state laser used to pump a Sirah Matisse TS Ti:Sapphire ring laser, producing ∼1 W of 744 nm light with 10 W of pump-laser power. A Spectra-Physics WaveTrain was used to generate 372 nm light by frequency doubling the 744 nm light. The 372 nm laser light was attenuated and stabilized at 300 μW using a laser power controller [29] with a ±0.05% power fluctuation. The diameter and focus of the laser light was adjusted using an optical telescope to be slowly converging at the photon detection region with a diameter of 0.9 mm at the focus measured by a CCD camera. The transmission of laser light through the CLS beam line was 87%. A typical photon background rate was 10^5/s, of which 3×10^4/s was due to beam-related background from the charge-exchange process, and the rest resulted from scattered laser light.

A scanning voltage was applied to the CEC to tune the Doppler-shifted laser frequency into resonance with the hyperfine transitions. This voltage was measured using a 1000:1 voltage divider calibrated to an accuracy of 1×10^{-4}, and was recorded 10 times each second using a digital voltmeter, in order to ensure that a measurement was taken at each voltage step during the scan. The total ion beam energy relevant for the laser excitation is given by the difference between applied potentials to the CEC and the RFQ, which were recorded into the data files and used in the analysis. The laser frequency was set to 26 904.1500 cm^{-1} to cover the isotope shifts and hyperfine spectra of ^{53,56}Fe within a ±2 kV scanning voltage applied to the CEC. The laser wavelength was determined by measuring the fundamental frequency of the Ti:Sapphire laser light by a HighFinesse WSU30 [30], which was calibrated by a frequency-stabilized He-Ne laser, with an absolute accuracy of 30 MHz (3σ).

Ion beams of stable ^{56}Fe were produced using a Penning Ionization Gauge ion source [28] installed upstream of the RFQ cooler/buncher. Every few hours throughout the experiment, the radioactive ^{53}Fe beam was stopped and the ^{56}Fe beam was used for about an hour. The fluorescence spectrum of ^{56}Fe was measured as a reference to determine the resonance line shape and to monitor the time-dependent centroid shift of about 2 V due mainly to the temperature variation over a week running time. The number of ^{56}Fe ions in a bunch was limited to about 10^4 to keep a similar space charge condition in the trap as to radioactive beam measurements, but the data collection was done with a higher beam-bunch repetition rate of 30 Hz to efficiently collect calibration data. This different rate has no discernible impact on the data analysis.

IV. RESULT

A. Hyperfine spectrum

The measured fluorescence spectrum of the reference ^{56}Fe is shown in Fig. 4 as a function of laser frequency relative to an arbitrary frequency of 805 678.7330 GHz. The squares are data and the solid line is the best fit to the data. An asymmetric Voigt profile [31] was used for the fit to reproduce the asymmetric tail at the low-frequency side of resonance, due to inelastic processes in the atomic charge-exchange

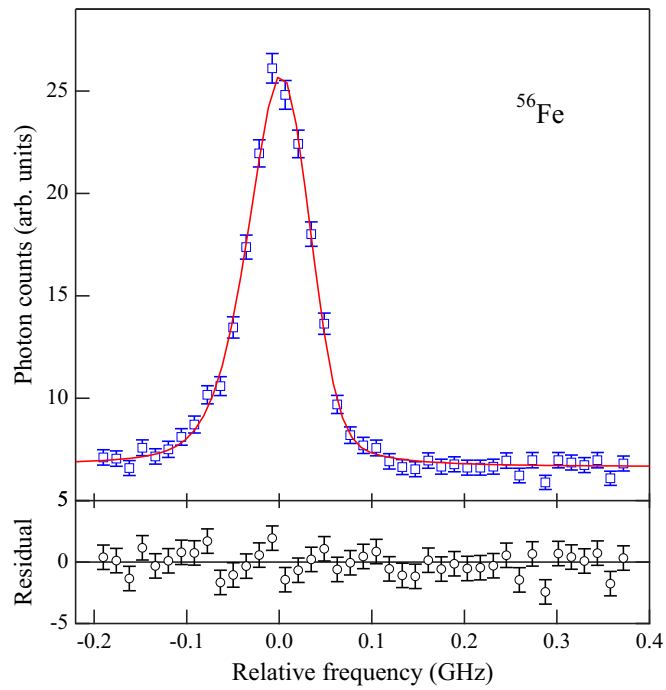

FIG. 4. The fluorescence spectrum of ^{56}Fe. The number of detected photons is plotted as a function of the relative laser frequency from an arbitrary value of 805 678.7330 GHz. The solid line is the best fit to the data using an asymmetric Voigt profile. The underlying plot shows the deviation from the fit line divided by the error of the data point.

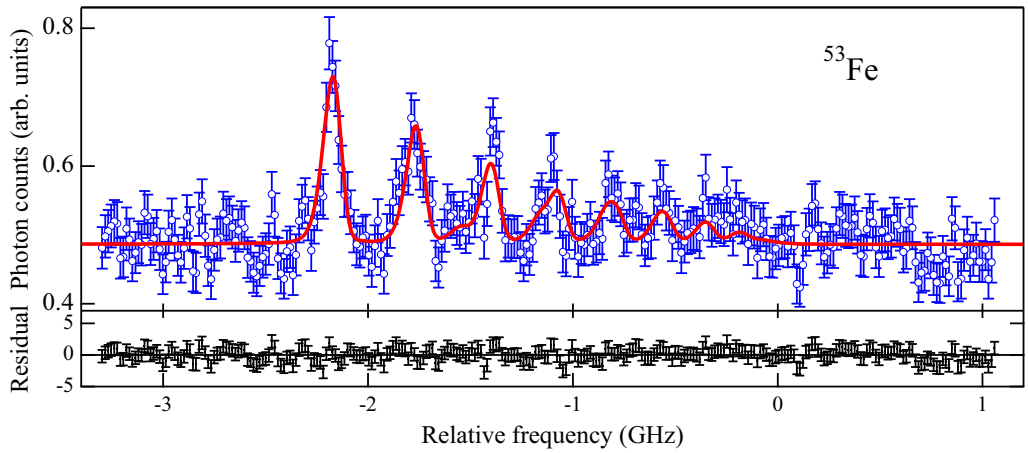

FIG. 5. The hyperfine spectrum of ^{53}Fe. The number of detected photons is plotted as a function of the relative laser frequency from an arbitrary value of 805 678.7330 GHz. The solid line is the best fit to the data using an asymmetric Voigt profile. The underlying plot shows the deviation from the fit line divided by the error of the data point.

reactions with sodium vapor [25,27]. The fitting parameter for the asymmetry was determined from the fit to the hyperfine spectrum of ^{56}Fe, which has high statistics and contains a single resonance peak with no hyperfine splitting. The asymmetry was then held constant in the fits for hyperfine spectrum of ^{53}Fe. The measured hyperfine spectrum of ^{53}Fe is shown in Fig. 5. The hyperfine spectrum of the $3d^64s^2\ ^5D_4 \leftrightarrow 3d^64s4p\ ^5F_5$ transition contains 21 allowed hyperfine transitions. All transitions are taken into account in the fit, and some of the peaks overlap and make line shapes appear broader. A small fluctuation of the high voltage that determined the ion beam energy over a few days data accumulation time resulted in a broader line width of ^{53}Fe than that of ^{56}Fe. The line width of the asymmetric Voigt profile was therefore kept as a free fitting parameter in the fit of the ^{53}Fe hyperfine spectrum. Relative intensities among these peaks were fixed in the fits based on angular momentum dependent factors in the reduced transition probabilities. The fitting functions reproduce the data well with a normalized chi square of $\chi^2/\nu = 1.00$. The contaminating isomeric state of ^{53m}Fe in the ^{53}Fe beam did not affect the measured hyperfine spectra due to the small fraction of the isomeric state. The hyperfine pumping effects were not observed at the statistical level of the current data and were not taken into account in the fit.

B. Magnetic-dipole hyperfine coupling constant

The ratio $A^{\rm HF}(^5F_5)/A^{\rm HF}(^5D_4) = 2.15(2)$ is known for stable ^{57}Fe [32] and was held constant in the fit of the ^{53}Fe hyperfine spectrum. The hyperfine anomaly [18] is not known for Fe isotopes but is typically smaller than the uncertainty of 1% in the present result of the magnetic moment, and is therefore neglected in the present analysis. The magnetic-dipole hyperfine coupling constant was obtained as

$$A^{\rm HF}(^5D_4) = -39.2(4)(6)\,{\rm MHz}. \quad (6)$$

The second uncertainty of $A^{\rm HF}$ is a systematic contribution that arises from the uncertainty on the ratio of $A^{\rm HF}$ between $^5D_4$ and $^5F_5$ states. The magnetic moment of ^{53}Fe can be deduced from Eq. (4) together with the $A^{\rm HF}(^5D_4)$ for ^{53}Fe and ^{57}Fe, and the magnetic moment of ^{57}Fe as

$$\mu(^{53}{\rm Fe}) = \mu(^{57}{\rm Fe})\frac{A^{\rm HF}(^{53}{\rm Fe})}{A^{\rm HF}(^{57}{\rm Fe})}\frac{I(^{53}{\rm Fe})}{I(^{57}{\rm Fe})}. \quad (7)$$

Using values of $A^{\rm HF}(^{57}{\rm Fe}) = +38.0795(10)\,{\rm MHz}$ [33], $\mu(^{57}{\rm Fe}) = +0.09062300(9)\,\mu_N$ [34,35], $I(^{53}{\rm Fe}) = 7/2$, and $I(^{57}{\rm Fe}) = 1/2$, the magnetic moment of ^{53}Fe was deduced to be

$$\mu(^{53}{\rm Fe}) = -0.65(1)\,\mu_N, \quad (8)$$

where the statistical and systematic uncertainties on the $A^{\rm HF}(^{53}{\rm Fe})$ were added quadratically. The results are summarized in Table I.

TABLE I. Magnetic moment of ^{53}Fe. The present result and theoretical calculations including the $T = 1/2$ mirror partner ^{53}Co are summarized. The isoscalar spin expectation values are also listed.

	^{53}Fe	^{53}Co	
I^π	$\frac{7}{2}^-$	$\frac{7}{2}^-$	
$A^{\rm HF}(^5D_4)$ (MHz)	−39.2(4)(6)		
	$\mu\ (\mu_N)$		$\langle\sum\sigma\rangle$
Present	−0.65(1)		
Single particle	−1.913	+2.793	1
Shell model			
Full fp $g^{\rm free}$	−0.51	+4.34	0.87
Full fp $g^{\rm eff}$	−0.66	+4.42	0.68
Buck-Perez systematics			
β-decay lifetime	−0.64(9)	+4.54(11)	1.05(37)
Mirror μ[a]		+4.55(5)	1.05(13)

[a]Present $\mu(^{53}{\rm Fe})$ was used to deduce $\mu(^{53}{\rm Co})$, and these μs were used to obtain $\langle\sum\sigma\rangle$.

TABLE II. Magnetic field and electric field gradient of $^5D_4$ and $^5F_5$ states in Fe I calculated using the MCDF method. The adopted values were used for the extraction of Q. The experimental values for $B(0)$ were obtained from A^{HF} [33] and μ [34] of ^{57}Fe.

		$B(0)$ (MHz/μ_N)		q (MHz/fm^2)		
	ΔE (cm^{-1})	$^5D_4$	$^5F_5$	$^5D_4$	$^5F_5$	Ref.
Model I	24805	1274	2328	585	734	
Model II	26462	1274	2310	581	738	
Model III	26392	1274	2328	590	745	
+ single excitations	25432	798	2065	573	783	
experiment	26874.550	840.39(2)	2254(24)			[33,34]
adopted				590(90)	745(100)	

C. Electric-quadrupole hyperfine coupling constant

Both the B^{HF}s for $^5D_4$ and $^5F_5$ states were kept as free parameters in the fit of the ^{53}Fe hyperfine spectrum, and obtained as

$$B^{\mathrm{HF}}(^5D_4) = +200(90)\,\mathrm{MHz}, \quad (9)$$

$$B^{\mathrm{HF}}(^5F_5) = +260(100)\,\mathrm{MHz}. \quad (10)$$

No B^{HF} nor quadrupole moment is known for any other Fe isotope, therefore the procedure of using a reference isotope [Eq. (5)], as for the deduction of the magnetic moment, cannot be applied here. In the absence of known electric field gradients for $q(^5D_4)$ and $q(^5F_5)$, these values were computed using the multiconfiguration Dirac-Fock (MCDF) method [36] as implemented in the GRASP2K package [37]. The wave function expansion is generated by the active space method, where virtual single and double excitations into several layers of correlation orbitals are used to approximate the dominant electron correlation effects and to monitor the convergence of the observables. All computations were started from a common set of occupied (spectroscopic) orbitals to ensure the balance between the upper and lower level. The active space was then systematically enlarged by adding several correlation layers that were separately optimized for the $3d^64s^2\ ^5D_4$ ground level and the excited $3d^64s4p\ ^5F_5$ level.

Several independent calculations were carried out to estimate the uncertainty and the convergence behavior of the magnetic field and the electric field gradient. Model I is a single reference calculation, where virtual excitations from the ground and excited configurations into correlation orbitals with angular momentum $l \leqslant 4$ were used, which yielded unbalanced results as the transition energy is significantly too low. The computation labeled Model II was constructed from a multi-reference set that additionally contained the $3d^64p^2$ configuration for the ground level and $3d^74p$ for the excited level. Due to computational restrictions, it was only possible to optimize three correlation layers for these two models. Restricting the angular momentum of the correlation layers to a maximum of $l = 3$ allowed the optimization of a fourth layer (the Model III). The variation due to the restriction in the angular momentum was found to be negligible, which confirms the saturation of the computations with respect to the valence-valence correlation.

Results obtained from the three previously introduced computational models are summarized in Table II, together with calculations of the magnetic field as a benchmark. While the calculated magnetic field $B(0)$ for the excited $^5F_5$ state agrees well with the experimental value, the value for the $^5D_4$ ground state does not match with the experimental value. This deviation is due to the correlation with the core, that was kept closed in the computational Models I through III. Several tests were performed for the ground level, where the core was opened for double excitations into one correlation layer optimized on top of the zero-order approximation. It was found that the $2s$ shell has a significant contribution to the magnetic field. However, it was not possible to saturate the calculations, though the electric field gradient does not deviate more than 15% from the adopted value. Additionally, a series of calculations with purely single excitations from all shells, except $1s$, to nine correlation layers was performed for both levels. These computations converged to magnetic field values of 715 MHz and 1960 MHz for the ground and excited level, respectively. An agreement with experimental values of about 15% is achieved for both levels, and resolves the above discrepancy due to neglected core correlation for the ground level. The results for the electric field gradient q obtained from the same models based on purely single excitations for the ground and excited levels are 573 MHz/fm^2 and 783 MHz/fm^2, respectively. These computed values agree with Models I through III within 5%. Adding these single excitations to Model III, we arrive at the results in the fourth line of Table II. Here, again four correlation layers are optimized on top of the multireference zero-order solution. However, the results do not fully converge when extending the configuration space, hence the results of Model III are adopted for the evaluation of the quadrupole moment. Nevertheless, the magnetic field of the ground state is significantly reduced due to the core-polarization effect that is simulated by the single excitations and is now also in very good agreement with the experimental value. The corresponding values for the electric field gradient are again in an agreement of about 5% with the adopted value. Since the magnetic field is more sensitive to electron correlation effects, the deviation of the magnetic field is often taken as an upper limit of the error on the electric field gradients [38,39]. Therefore, an upper bound of 15% was conservatively taken as an uncertainty of

TABLE III. $B^{\rm HF}$ and nuclear quadrupole moment of ^{53}Fe. The values in the first and second parentheses in the bracket for the present Q are uncertainties due to $B^{\rm HF}$ and q, respectively. A quadratic sum was taken for the total uncertainty for each state.

		Q (e^2fm^2)	
State	$B^{\rm HF}$ (MHz)	Exp.	Theor.
$3d^6 4s^2\ ^5D_4$	+200(90)	+34(16) [(15)(5)]	
$3d^6 4s 4p\ ^5F_5$	+260(100)	+35(14) [(13)(5)]	
Average		+35(15)	+41

the computed electric field gradients. The obtained values were

$$q(^5D_4) = 590(90)\,\text{MHz/fm}^2, \tag{11}$$

$$q(^5F_5) = 745(100)\,\text{MHz/fm}^2. \tag{12}$$

The quadrupole moment can now be extracted from Eq. (3) as $Q(^{53}\text{Fe}) = +34(16)\,e^2\text{fm}^2$ and $+35(14)\,e^2\text{fm}^2$ from $B^{\rm HF}$ of the $^5D_4$ and $^5F_5$ states, respectively.

The calculated electric field gradients, and experimental $B^{\rm HF}$s of $^5D_4$ and $^5F_5$ states give consistent quadrupole moments. A simple average is conservatively taken for the final result as

$$Q(^{53}\text{Fe}) = +35(15)\,e^2\text{fm}^2. \tag{13}$$

The results are summarized in Table III.

V. DISCUSSION

A. Shell-model calculation

Shell model calculations were performed for the electromagnetic moments of ^{53}Fe ground state. They were carried out using a ^{40}Ca core in the full fp shell-model space with the GXPF1A effective interaction [11,40], which reproduces the shell structure around the mass region of interest, using the NUSHELLX package [40].

The magnetic moment operator used in the present calculation is

$$\boldsymbol{\mu} = g_s \boldsymbol{s} + g_l \boldsymbol{l}, \tag{14}$$

where g_s and g_l are the spin and the orbital g factors, respectively. The free nucleon g factors ($g_l^{\rm p} = 1$, $g_l^{\rm n} = 0$, $g_s^{\rm p} = 5.586$, and $g_s^{\rm n} = -3.826$) and effective g factors [11] ($g_s^{\rm eff} = 0.9 g_s^{\rm free}$, and $g_l = 1.1$ and -0.1 for protons and neutrons, respectively) were used for the calculation. These results are summarized in Table I. The single particle value ($\mu = -1.913\,\mu_N$) significantly overestimates the absolute value of the magnetic moment and indicates a sizable contribution from configuration mixing. The probability of the lowest-order single particle configuration $\pi(1f_{7/2})^6\nu(1f_{7/2})^7$ in the ground state wave function of ^{53}Fe is calculated to be ~50%, which is consistent with that of ~60% of the closed-shell ^{56}Ni ground state [11]. The calculation with effective g factors ($\mu = -0.66\,\mu_N$) best reproduces the present magnetic moment.

For the calculation of the electric-quadrupole moment, the effective charges $e_{\rm p} = 1.5$ and $e_{\rm n} = 0.5$ were adopted [11]. The obtained value $Q = +41\,e^2\text{fm}^2$ shows good agreement with the quadrupole moments obtained here and listed in Table III, including its prolate deformation (sign). It is noted that the electric field gradient was reliably calculated for the complex electronic system of the Fe atom to help deduce quadrupole moments, though the present result is dominated by the statistical uncertainty. The good agreements of present results with the shell model calculations support the soft nature of ^{56}Ni [11].

B. Buck-Perez systematic relation

The magnetic moments of the isospin $T = 1/2$ mirror nuclei can be expressed [17], assuming charge symmetry of nuclear forces, as

$$\boldsymbol{\mu_p} = g_l^{\rm p}\boldsymbol{l_o} + g_s^{\rm p}\boldsymbol{s_o} + g_l^{\rm n}\boldsymbol{l_e} + g_s^{\rm n}\boldsymbol{s_e}, \tag{15}$$

$$\boldsymbol{\mu_n} = g_l^{\rm n}\boldsymbol{l_o} + g_s^{\rm n}\boldsymbol{s_o} + g_l^{\rm p}\boldsymbol{l_e} + g_s^{\rm p}\boldsymbol{s_e}, \tag{16}$$

where the $\mu_{p/n}$ denotes the odd-proton and odd-neutron members of a mirror pair. The subscripts o and e represent contributions from odd and even groups, respectively, to the angular momentum and spin operators. The $T = 1/2$ mirror magnetic moments can be directly correlated from Eqs. (15) and (16) as

$$\gamma_p + \Delta\gamma_p = \alpha(\gamma_n + \Delta\gamma_n) + \beta, \tag{17}$$

where γ is the gyromagnetic ratio (μ/I), α and β are constants containing the g factors, and $\Delta\gamma$ is a small correction from the even nucleon group, which is calculated by theory [17]. Using known mirror magnetic moments of $T = 1/2$ pairs, $\alpha = -1.147(13)$ and $\beta = 1.027(13)$ were obtained [17]. The present result $\mu(^{53}\text{Fe})$ [$\gamma_n = -0.186(3)$] and calculated $\Delta\gamma_n = -0.1431$ and $\Delta\gamma_p = 0.1053$ for ^{53}Fe and ^{53}Co, respectively, are used to obtain $\gamma_p = 1.30(1)$ for the $T = 1/2$ mirror partner ^{53}Co. This results in a predicted value of

$$\mu(^{53}\text{Co}) = +4.55(5)\,\mu_N. \tag{18}$$

A value of $\mu(^{53}\text{Co}) = +4.42(5)\,\mu_N$ is obtained without the even nucleon corrections. The predicted values are summarized in Table I. It is noted that a recent analysis [41] using an updated list of mirror magnetic moments was performed to obtain α and β without a contribution from the even nucleon group. The α and β are consistent with the ones discussed in [17].

The $T = 1/2$ mirror magnetic moments can also be correlated to the β-decay lifetime [17]. Using the log $ft = 3.625(17)$ [42] for the transition between ^{53}Co and ^{53}Fe, and $ft = 3072.27(72)$ s of $0^+ \to 0^+$ superallowed transitions [43], this correlation gives less precise predictions of both $\mu(^{53}\text{Fe}) = -0.64(9)\,\mu_{\rm N}$ and $\mu(^{53}\text{Co}) = +4.54(11)\,\mu_{\rm N}$ with the even nucleon corrections. The predicted magnetic moment of ^{53}Fe is consistent with the present result. The prediction for ^{53}Co is consistent with the value obtained from the correlation based on mirror magnetic moments, though the error bar is larger by a factor of two.

C. Isoscalar spin expectation value

The isoscalar spin expectation value $\langle\sum\sigma\rangle$ can be extracted from the sum of mirror magnetic moments [44]. A value of $\langle\sum\sigma\rangle$ for the $A = 53$, $T = 1/2$ mirror pair may be obtained using the present $\mu(^{53}\mathrm{Fe})$ and the systematic value of $\mu(^{53}\mathrm{Co})$ evaluated by the Buck-Perez relation. It is obtained as $\langle\sum\sigma\rangle = 1.05(13)$, whereas the theory predicts 0.68 and underestimates the experimental value as summarized in Table I.

A similar discrepancy was observed in the neighboring $A = 55$, $T = 1/2$ system [7], where $\langle\sum\sigma\rangle$ values were obtained as 0.91(7) and 0.65 for experiment and theory, respectively. The deviation is explained as a cancellation in $\langle\sum\sigma\rangle$ from contributions between the enhancement due to the large orbital angular momentum, and the reduction due to the configuration mixing. Such an enhancement can also be seen in the *sd* shell nuclei, and was explained by examining the isovector and isoscalar components of the $M1$ operator separately [45,46].

An evaluation of isoscalar components of the $M1$ operator in the fp shell is required to obtain isoscalar effective g factors that can explain the $\langle\sum\sigma\rangle$ obtained for $A = 55$ and inferred for $A = 53$. The experimental determination of $\mu(^{53}\mathrm{Co})$ is critical to further the discussion.

VI. SUMMARY

The bunched-beam collinear laser spectroscopy technique was applied for the first time to the ^{53}Fe beam prepared through projectile-fragmentation reactions followed by gas stopping. This novel scheme complements existing capabilities, for example of ISOL facilities, and opens new opportunities for laser spectroscopy to explore radioactive isotopes. The atomic hyperfine structure of the $3d^64s^2\,{}^5D_4 \leftrightarrow 3d^64s4p\,{}^5F_5$ transition in Fe I was measured for the ^{53}Fe isotope. The hyperfine magnetic and quadrupole coupling constants were determined from the hyperfine structure, and μ and Q of ^{53}Fe were extracted.

The known μ and A^{HF} of stable ^{57}Fe were used to extract the magnetic moment of ^{53}Fe as $\mu(^{53}\mathrm{Fe}) = -0.65(1)\,\mu_{\mathrm{N}}$. The electric field gradient of the Fe atom was calculated using the MCDF method to extract Q from B^{HF}, since no ground state Q or B^{HF} has been determined for any Fe isotopes so far. The quadrupole moment was obtained as $Q(^{53}\mathrm{Fe}) = +35(15)\ e^2\mathrm{fm}^2$. Shell model calculations with the GXPF1A interaction well reproduce the present μ and Q using typical effective g factors and effective charges in the fp shell, respectively. The good agreements support the soft nature of the ^{56}Ni nucleus.

The present $\mu(^{53}\mathrm{Fe})$ may be used to obtain a prediction on the magnetic moment of the $T = 1/2$ mirror partner ^{53}Co as $\mu(^{53}\mathrm{Co}) = +4.55(5)\,\mu_{\mathrm{N}}$, based on the Buck-Perez systematic relation. An isoscalar spin expectation value was inferred using the present $\mu(^{53}\mathrm{Fe})$ and the systematic value of $\mu(^{53}\mathrm{Co})$ as $\langle\sum\sigma\rangle = 1.05(13)$. The shell-model calculation with effective g factors used in the present study gives $\langle\sum\sigma\rangle = 0.68$ and does not reproduce the present value, which is very sensitive to small differences in the magnetic moments. The evaluation of isoscalar components in the fp shell is essential to obtain effective g factors that are more sensitive to details of nuclear structure in the region around ^{56}Ni. The measurement of $\mu(^{53}\mathrm{Co})$ is of importance to further the discussion.

ACKNOWLEDGMENTS

This work was supported in part by the National Science Foundation, Grants No. PHY-15-65546 and PHY-1404442; the U.S. Department of Energy, National Nuclear Security Administration, Grant No. DE-NA0002924; the U.S. Department of Energy, Office of Science, Office of Nuclear Physics, Grants No. DE-SC0013365, No. DE-AC02-06CH11357, and No. DE-AC05-00OR22725 with UT-Battelle, LLC; the German Research Foundation Contract No. SFB 1245; the German Federal Ministry of Education and Research (BMBF), Grants No. 05P12RFFTG and No. 015P15SJCIA.

[1] D. Warner, Nature **430**, 517 (2004).
[2] B. Bastin, S. Grévy, D. Sohler, O. Sorlin, Z. Dombrádi, N. L. Achouri, J. C. Angélique, F. Azaiez, D. Baiborodin, R. Borcea, C. Bourgeois, A. Buta, A. Bürger, R. Chapman, J. C. Dalouzy, Z. Dlouhy, A. Drouard, Z. Elekes, S. Franchoo, S. Iacob, B. Laurent, M. Lazar, X. Liang, E. Liénard, J. Mrazek, L. Nalpas, F. Negoita, N. A. Orr, Y. Penionzhkevich, Z. Podolyák, F. Pougheon, P. Roussel-Chomaz, M. G. Saint-Laurent, M. Stanoiu, I. Stefan, F. Nowacki, and A. Poves, Phys. Rev. Lett. **99**, 022503 (2007).
[3] R. V. F. Janssens, Nature **459**, 1069 (2009).
[4] D. Steppenbeck, S. Takeuchi, N. Aoi, P. Doornenbal, M. Matsushita, H. Wang, H. Baba, N. Fukuda, S. Go, M. Honma, J. Lee, K. Matsui, S. Michimasa, T. Motobayashi, D. Nishimura, T. Otsuka, H. Sakurai, Y. Shiga, P.-A. Söderström, T. Sumikama, H. Suzuki, R. Taniuchi, Y. Utsuno, J. J. Valiente-Dobón, and K. Yoneda, Nature **502**, 207 (2013).
[5] O. Sorlin and M. G. Porquet, Prog. Part. Nucl. Phys. **61**, 602 (2008).
[6] M. Honma, T. Otsuka, B. A. Brown, and T. Mizusaki, Phys. Rev. C **65**, 061301(R) (2002).
[7] J. S. Berryman, K. Minamisono, W. F. Rogers, B. A. Brown, H. L. Crawford, G. F. Grinyer, P. F. Mantica, J. B. Stoker, and I. S. Towner, Phys. Rev. C **79**, 064305 (2009).
[8] P. T. Callaghan, M. Kaplan, and N. J. Stone, Nucl. Phys. A **201**, 561 (1973).
[9] T. E. Cocolios, A. N. Andreyev, B. Bastin, N. Bree, J. Büscher, J. Elseviers, J. Gentens, M. Huyse, Y. Kudryavtsev, D. Pauwels, T. Sonoda, P. V. den Bergh, and P. V. Duppen, Phys. Rev. Lett. **103**, 102501 (2009).
[10] T. Ohtsubo, D. J. Cho, Y. Yanagihashi, S. Ohya, and S. Muto, Phys. Rev. C **54**, 554 (1996).
[11] M. Honma, T. Otsuka, B. A. Brown, and T. Mizusaki, Phys. Rev. C **69**, 034335 (2004).

[12] K. Minamisono, D. M. Rossi, R. Beerwerth, S. Fritzsche, D. Garand, A. Klose, Y. Liu, B. Maaß, P. F. Mantica, A. J. Miller, P. Müller, W. Nazarewicz, W. Nörtershäuser, E. Olsen, M. R. Pearson, P. G. Reinhard, E. E. Saperstein, C. Sumithrarachchi, and S. V. Tolokonnikov, Phys. Rev. Lett. **117**, 252501 (2016).
[13] D. J. Morrissey, B. M. Sherrill, M. Steiner, A. Stolz, and I. Wiedenhoever, Nucl. Instrum. Meth. Phys. Res. B **204**, 90 (2003).
[14] K. Cooper, C. Sumithrarachchi, D. Morrissey, A. Levand, J. Rodriguez, G. Savard, S. Schwarz, and B. Zabransky, Nucl. Instrum. Meth. Phys. Res. A **763**, 543 (2014).
[15] R. Neugart, J. Billowes, M. L. Bissell, K. Blaum, B. Cheal, K. T. Flanagan, G. Neyens, W. Nörtershäuser, and D. T. Yordanov, J. Phys. G Part. Phys. **44**, 064002 (2017).
[16] P. Dendooven, Nucl. Instrum. Meth. Phys. Res. B **126**, 182 (1996).
[17] S. M. Perez, W. A. Richter, B. A. Brown, and M. Horoi, Phys. Rev. C **77**, 064311 (2008).
[18] J. R. Persson, At. Data Nucl. Data Tables **99**, 62 (2013).
[19] K. Minamisono, P. F. Mantica, A. Klose, S. Vinnikova, A. Schneider, B. Johnson, and B. R. Barquest, Nucl. Instrum. Meth. Phys. Res. A **709**, 85 (2013).
[20] D. M. Rossi, K. Minamisono, B. R. Barquest, G. Bollen, K. Cooper, M. Davis, K. Hammerton, M. Hughes, P. F. Mantica, D. J. Morrissey, R. Ringle, J. A. Rodriguez, C. A. Ryder, S. Schwarz, R. Strum, C. Sumithrarachchi, D. Tarazona, and S. Zhao, Rev. Sci. Instrum. **85**, 093503 (2014).
[21] B. R. Barquest, G. Bollen, P. F. Mantica, K. Minamisono, R. Ringle, and S. Schwarz, Nucl. Instrum. Meth. Phys. Res. A **866**, 18 (2017).
[22] See http://www.ohm-labs.com for information on the HVS-100 voltage divider (accessed in 2017).
[23] P. Campbell, H. L. Thayer, J. Billowes, P. Dendooven, K. T. Flanagan, D. H. Forest, J. A. R. Griffith, J. Huikari, A. Jokinen, R. Moore, A. Nieminen, G. Tungate, S. Zemlyanoi, and J. Äystö, Phys. Rev. Lett. **89**, 082501 (2002).
[24] A. Nieminen, P. Campbell, J. Billowes, D. H. Forest, J. A. R. Griffith, J. Huikari, A. Jokinen, I. D. Moore, R. Moore, G. Tungate, and J. Äystö, Phys. Rev. Lett. **88**, 094801 (2002).
[25] A. Klose, K. Minamisono, C. Geppert, N. Frömmgen, M. Hammen, J. Krämer, A. Krieger, C. D. P. Levy, P. F. Mantica, W. Nörtershäuser, and S. Vinnikova, Nucl. Instrum. Meth. Phys. Res. A **678**, 114 (2012).
[26] T. R. O'Brian, M. E. Wickliffe, J. E. Lawler, W. Whaling, and J. Brault, J. Opt. Soc. Am. B **8**, 1185 (1991).
[27] A. Klose, K. Minamisono, and P. F. Mantica, Phys. Rev. A **88**, 042701 (2013).
[28] C. A. Ryder, K. Minamisono, H. B. Asberry, B. Isherwood, P. F. Mantica, A. Miller, D. M. Rossi, and R. Strum, Spectroch. Acta Part B **113**, 16 (2015).
[29] See http://www.brocktoneo.com for information on the laser-power controller (accessed in 2016).
[30] See http://www.highfinesse.com for information on the wavelength meter (accessed in 2016).
[31] A. L. Stancik and E. B. Brauns, Vibrat. Spectrosc. **47**, 66 (2008).
[32] S. Krins, S. Oppel, N. Huet, J. von Zanthier, and T. Bastin, Phys. Rev. A **80**, 062508 (2009).
[33] W. J. Childs and L. S. Goodman, Phys. Rev. **148**, 74 (1966).
[34] W. Sahm and A. Schwenk, Z. Naturforsch. **29a**, 1763 (1974).
[35] N. Stone, At. Data Nucl. Data Tables **90**, 75 (2005).
[36] I. P. Grant, *Relativistic Quantum Theory of Atoms and Molecules: Theory and Computation* (Springer Science & Business Media, New York, 2007), Vol. 40.
[37] P. Jönsson, X. He, C. F. Fischer, and I. P. Grant, Comput. Phys. Commun. **177**, 597 (2007).
[38] J. Bieroń, C. F. Fischer, S. Fritzsche, G. Gaigalas, I. P. Grant, P. Indelicato, P. Jönsson, and P. Pyykkö, Phys. Scr. **90**, 054011 (2015).
[39] J. Bieroń and P. Pyykkö, Phys. Rev. Lett. **87**, 133003 (2001).
[40] M. Honma, T. Otsuka, B. A. Brown, and T. Mizusaki, Eur. Phys. J. A **25, s01**, 499 (2005).
[41] T. J. Mertzimekis, Phys. Rev. C **94**, 064313 (2016).
[42] A. Kankainen, V. V. Elomaa, T. Eronen, D. Gorelov, J. Hakala, A. Jokinen, T. Kessler, V. S. Kolhinen, I. D. Moore, S. Rahaman, M. Reponen, J. Rissanen, A. Saastamoinen, C. Weber, and J. Äystö, Phys. Rev. C **82**, 034311 (2010).
[43] J. C. Hardy and I. S. Towner, Phys. Rev. C **91**, 025501 (2015).
[44] K. Sugimoto, Phys. Rev. **182**, 1051 (1969).
[45] B. A. Brown and B. H. Wildenthal, Phys. Rev. C **28**, 2397 (1983).
[46] B. A. Brown and B. H. Wildenthal, Nucl. Phys. A **474**, 290 (1987).